Sun, Z., Jian, Z., Stock, J.M., Larsen, H.C., Klaus, A., Alvarez Zarikian, C.A., and the Expedition 367/368 Scientists

Proceedings of the International Ocean Discovery Program Volume 367/368 publications.iodp.org



https://doi.org/10.14379/iodp.proc.368X.101.2020



Expedition 368X summary¹

L.B. Childress, C.A. Alvarez Zarikian, A. Briais, K.A. Dadd, J.-M. Deng, T.W. Höfig, X.-L. Huang, B. Li, J. Lin, C. Liu, Z. Liu, M.F.R. Nirrengarten, D.W. Peate, N. Qiu, S. Satolli, J.M. Stock, Z. Sun, F.M. van der Zwan, R. Xiang, L. Yi, and L. Zhong²

Keywords: International Ocean Discovery Program, IODP, JOIDES Resolution, Expedition 367, Expedition 368, Expedition 368X, South China Sea Rifted Margin, Site U1503, northern South China Sea, rifted margin, continent-ocean transition zone, hyperextension, continental breakup, lithosphere thinning, outer margin high, embryonic ocean

Contents

- **Abstract**
- 2 Introduction
- 3 Background
- **6** Expedition objectives
- 6 Coring and logging strategy
- 7 Site U1503 summary
- 15 Preliminary scientific assessment
- 15 References

Abstract

International Ocean Discovery Program (IODP) Expedition 368X is the third of three expeditions that form the South China Sea Rifted Margin program. Expeditions 367, 368, and 368X share the common key objectives of testing scientific hypotheses of breakup of the northern South China Sea (SCS) margin and comparing its rifting style and history to other nonvolcanic or magma-poor rifted margins. Seismic profiles across the margin in the IODP study area show from continent to ocean a wide extended continental margin, an outer margin high (OMH), and a continent-ocean transition (COT) zone displaying different ridges of unknown nature. Four primary sites were selected for the overall program: one in the OMH and three seaward of the OMH on distinct, margin-parallel basement ridges informally labeled Ridges A, B, and C from north to south. The ridges are located in the COT zone ranging from the OMH to the interpreted steady-state oceanic crust of the SCS. The main scientific objectives include

- 1. Determining the nature of the basement in crustal units across the COT of the SCS that are critical to constrain the style of
- 2. Constraining the time interval from initial crustal extension and plate rupture to the initial generation of igneous ocean crust,
- 3. Constraining vertical crustal movements during breakup, and
- 4. Examining the nature of igneous activity from rifting to seafloor spreading.

Also, sediment cores from the drill sites targeting primarily tectonic and basement objectives will provide information on the Cenozoic regional environmental development of the Southeast Asia margin.

Expedition 368X was planned to reoccupy a site started during Expedition 368. Because of repeated breakdowns of the low clutch diaphragm in the drawworks, Hole U1503A was abandoned after installing casing to 991.5 m. Despite this setback to Expedition 368 and the South China Sea Rifted Margin program, Hole U1503A was completed during Expedition 368X. The overarching scientific goal of Expeditions 367 and 368 was to unveil the mechanisms of continental breakup at the northern SCS margin from rifting through steady-state spreading. A key operational objective of Site U1503 was to sample the lowermost ~300 m of sediments on top of basement to constrain the age and subsidence history of the crust at this location, the timing of normal faulting, and the environment of the early half-graben fill. A second important goal was to sample at least 100 m of the igneous basement. A deep representative sampling of the igneous material at this site will provide an important reference frame for the modeling of breakup and early ocean spreading.

In Hole U1503A, the sediment sequence was cored with the rotary core barrel (RCB) system from 995.1 to 1597.84 m (602.74 m penetration; 128.01 m recovered; 21%) and then the underlying basement was continuously cored from 1597.84 to 1710.1 m (112.26 m penetration; 47.91 m recovered; 43%). Although logging deeper than 991.5 m (bottom of casing) was not possible because of unstable hole conditions, Hole U1503A was logged with the Versatile Seismic Imager in the cased portion of the hole. No days were lost to waiting on weather, and the only mechanical downtime was a 1.5 h period when an electrical malfunction caused the top drive to shut down for repairs.

Expedition 368X completed the operational objectives in Hole U1503A that were started during Expedition 368. In the SCS margin science program, material recovered during Expedition 368X will



¹ Childress, L.B., Alvarez Zarikian, C.A., Briais, A., Dadd, K.A., Deng, J.-M., Höfig, T.W., Huang, X.-L., Li, B., Lin, J., Liu, C., Liu, Z., Nirrengarten, M.F.R., Peate, D.W., Qiu, N., Satolli, S., Stock, J.M., Sun, Z., van der Zwan, F.M., Xiang, R., Yi, L., and Zhong, L., 2020. Expedition 368X summary. In Sun, Z., Jian, Z., Stock, J.M., Larsen, H.C., Klaus, A., Alvarez Zarikian, C.A., and the Expedition 367/368 Scientists, South China Sea Rifted Margin. Proceedings of the International Ocean Discovery Program, 367/368: College Station, TX (International Ocean Discovery Program, 367/368: College Station, 367/3 gram). https://doi.org/10.14379/iodp.proc.368X.101.2020

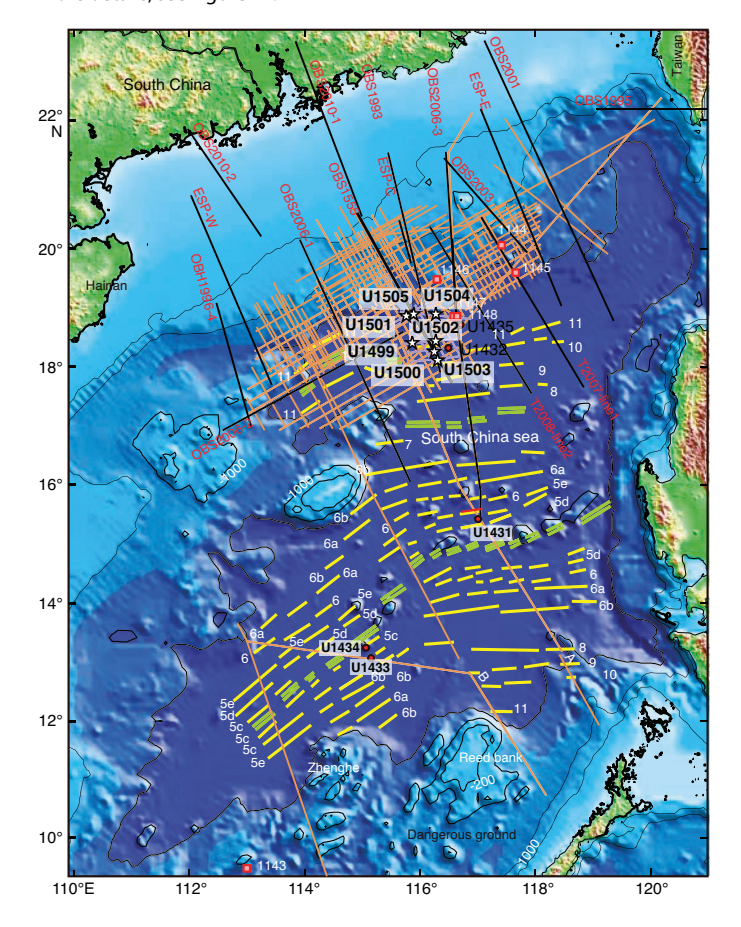
² Expedition 367/368 Scientists' affiliations.

contribute toward meeting the four specific objectives of Expeditions 367 and 368. Postcruise research on the sediments and basalt recovered from Hole U1503A will allow for determination of emplacement age, geochemical analyses of rock composition, and assessment of melting processes and age of crystallization. The combination of such analyses will contribute to geochemical or thermomechanical modeling that will constrain mantle origin and melting processes leading to the formation of these basalts.

Introduction

The South China Sea (SCS) margin (Figures F1, F2, F3) is an accessible and well-imaged location where drilling of synrift sediments and underlying basement will provide key constraints on the processes of rifting and eventual rupturing of the continental lithosphere during breakup at a highly extended rifted margin. International Ocean Discovery Program (IODP) Expeditions 367, 368, and 368X were based on drilling Proposals 878-CPP, 878-Add, 878-Add2, and 878-Add3. This project was implemented as a single science program, initially with 114 days of drilling operations spread across two IODP expeditions, as outlined in the Expedition 367/368 *Scientific Prospectus* (Sun et al., 2016b). A deep representative sampling of the basaltic material at Site U1503 would have provided an

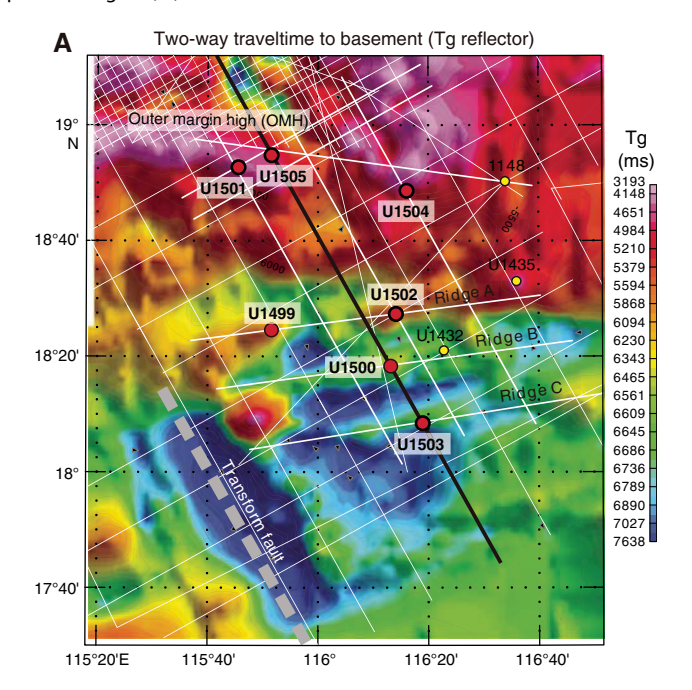
Figure F1. Seismic data coverage and magnetic anomalies of the South China Sea basin, Expeditions 367, 368, and 368X. Black lines = ocean-bottom seismometer (OBS) refraction data. Other seismic lines are mostly multichannel seismic reflection data. Yellow lines = magnetic isochrons from Briais et al. (1993). White stars = Expedition 367, 368, and 368X drill sites, red squares = ODP Leg 184 sites, red circles = IODP Expedition 349 sites. For more details, see Figure F2.



important reference frame for the modeling of continental breakup; however, planned operational objectives in Hole U1503A were not achieved during Expedition 368.

Expedition 368 installed a reentry system and 991.5 m of casing (10% inch) in Hole U1503A, but the hole could not be deepened

Figure F2. Two-way traveltime to (A) acoustic basement (Tg reflector) and (B) Unconformity T60 with Expedition 367, 368, and 368X sites. Proposed drilling transect (thick black line) was located approximately at the center of a margin segment bounded to the southwest by a transform fault. Northeastern boundary of the margin segment is located around IODP Expedition 349 Site U1435. In this location, the OMH and Ridge A seem to coalesce, and Ridges B and C of the COT become indistinct toward the northeast in the next margin segment. Note that the OMH is slightly oblique to the more parallel Ridges A, B, and C.



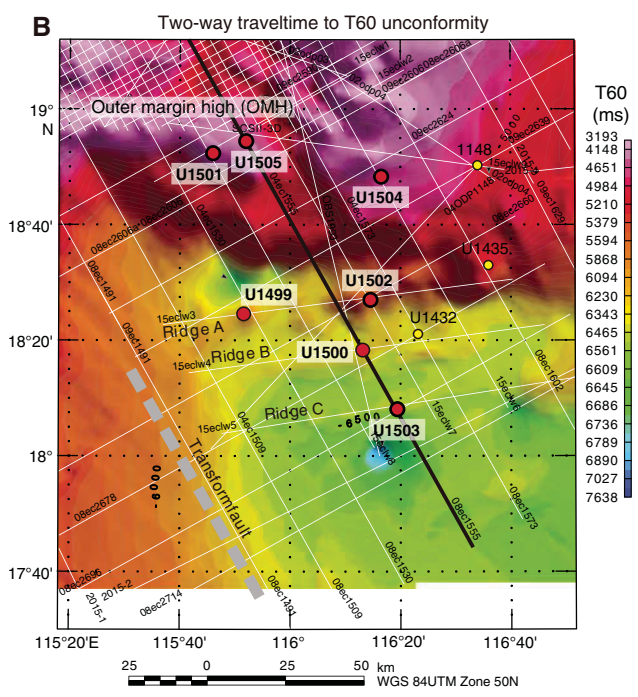
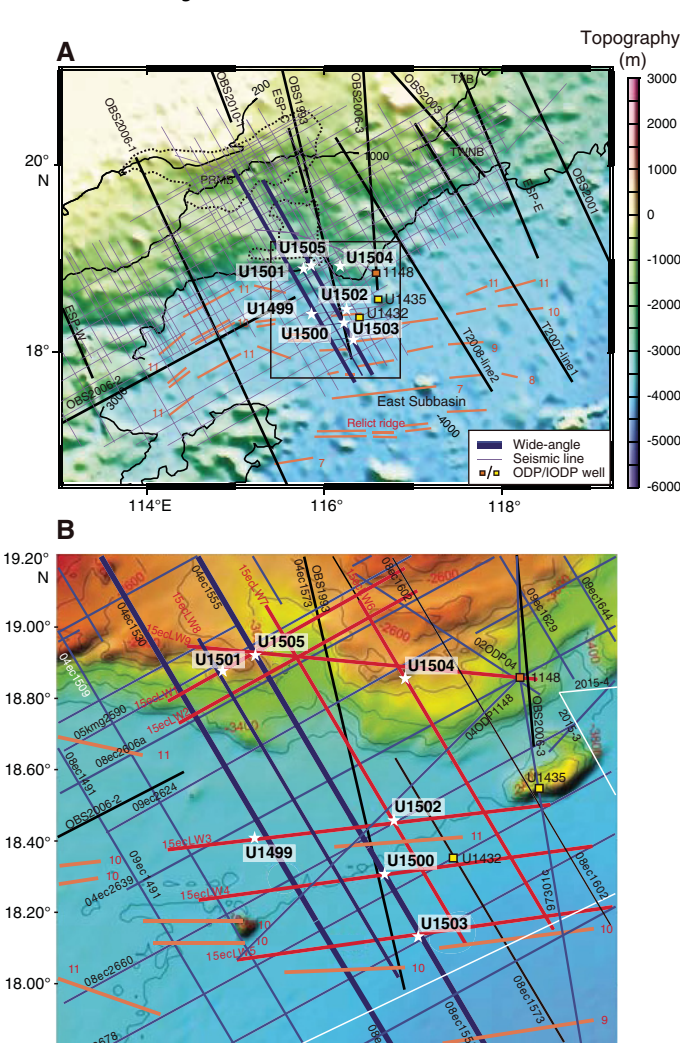


Figure F3. Bathymetric maps showing Expedition 367, 368, and 368X sites (stars) and (A) regional and (B) local coverage of 2-D, time-migrated multichannel seismic reflection seismic data and OBS data. Orange lines = magnetic isochrons from Briais et al. (1993), thick blue lines = key seismic lines used for planning of the drilling transect, red lines = other important seismic lines near the drilling sites.



because of mechanical problems with the drawworks, including a fourth clutch diaphragm failure and a breakdown of the aft shaft bearing on one of the Elmagco brakes. The continuing failures of the low clutch diaphragm and the lack of available spares to last until the end of the expedition limited the operation of the ship's drilling equipment to shallower than 3400 m water depth. Therefore, Site U1503 was abandoned without achieving the scientific objectives. Before departing Site U1503 during Expedition 368, the reentry system in Hole U1503A was inspected with the subsea camera. The cone appeared to be 1–2 m below the seafloor but was clearly visible and expected to be available for reentry at a later date. Expedition 368X was able to take advantage of a unique opportunity in

116.20°

3000

Bathymetry (m)

116.40°

116.60°

116.80°

115.80° 116.00°

17.80

115.40°E 115.60°

the R/V JOIDES Resolution schedule that resulted from forced equipment repairs. Expedition 368X added 20 days of drilling operations to the SCS margin science program. The drilling strategy for Expedition 368X was to finish the Expedition 368 Hole U1503A operational objectives, including coring the lowermost sediment and basement and logging the hole. During Expedition 368X, the sediment sequence was cored with the rotary core barrel (RCB) system from 995.1 to 1597.84 m (602.74 m penetration; 128.01 m recovered; 21%) and then the underlying basalt was continuously cored from 1597.84 to 1710.1 m (112.26 m penetration; 47.91 m recovered; 43%). Although logging deeper than 991.5 m (bottom of casing) was not possible because of unstable hole conditions, Hole U1503A was logged with the Versatile Seismic Imager (VSI) in the cased portion of the hole.

Background

Global questions regarding the formation of rifted margins

The Ocean Drilling Program (ODP; 1985–2003) made a major effort to understand the processes of continental breakup along the rifted margins of the North Atlantic (ODP Legs 103, 104, 149, 152, 163, 173, and 210). This effort resulted in the recognition of two end-members of rifted margins (see a summary of observations in Sun et al., 2016a, 2016b).

The first recognized end-member is volcanic rifted margins, examples of which are characterized by voluminous igneous activity in a relatively short time ($\sim 1-3$ My) during breakup and initial seafloor spreading; the pair of conjugate margins of Greenland and northwest Europe is an example of this type. In these locations, the asthenospheric mantle may have been anomalously hot (e.g., close to mantle plumes), which could have led to a thermal weakening of the continental lithosphere followed by rapid plate rupture.

The second recognized end-member is magma-poor rifted margins, which are interpreted to endure hyperextension of the continental crust, with tectonic extension at the distal margin eventually exhuming the subcontinental mantle lithosphere and leading to serpentinization of the mantle. The Newfoundland and Iberia pair of conjugate margins, where serpentinite basement occupies a broad area in the continent-ocean transition (COT) zone, is an example of this type of margin and is the only conjugate margin pair where this interpretation has been confirmed by scientific drilling. The introduction of water into the subcontinental lithospheric mantle is interpreted to have taken place through deep, crust-cutting faults, causing serpentinization that profoundly weakens the mantle lithosphere and facilitates plate rupture. The subsequent ultraslow spreading led to the exhumation of additional serpentinite on the seafloor (e.g., Dick et al., 2003) until sufficient magma production allowed for the formation of normal oceanic crust.

Elsewhere, other examples of highly extended rifted margins have been identified in seismic reflection data (e.g., Brune et al., 2017; Doré and Lundin, 2015), but it is not known if serpentinized mantle plays a critical role in all cases. Modeling by Huismans and Beaumont (2008, 2011) suggested several scenarios for the formation of rifted margins in the absence of anomalously hot asthenospheric mantle. One scenario (Type I of Huismans and Beaumont, 2011) is the Iberia-Newfoundland-type margin described above. In this case, lithospheric thinning initially occurs in the (upper) crust and extensional faults profoundly thin the continental crust (hyperextension) and eventually reach the mantle and cause serpentinization (Whitmarsh et al., 2001; Pérez-Gussinyé and Reston, 2001;

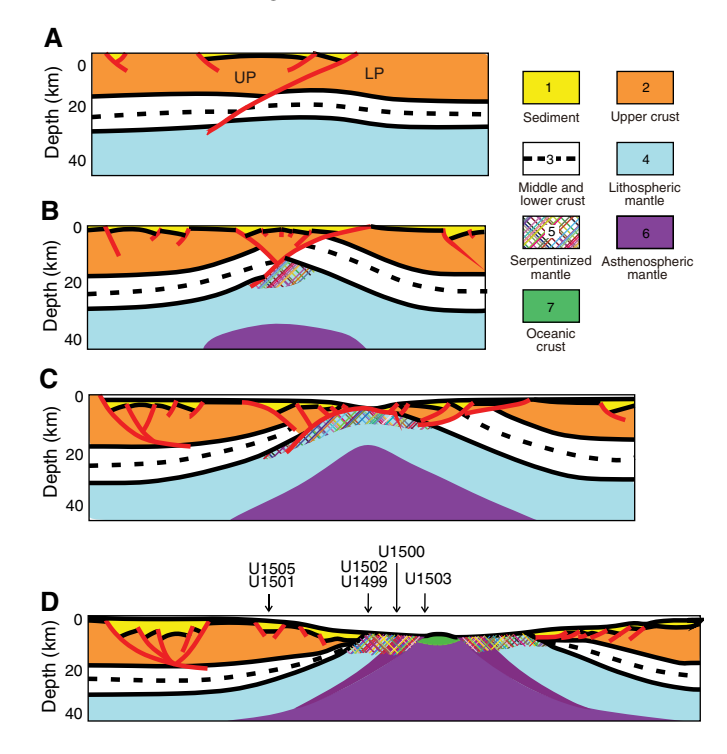
Pérez-Gussinyé et al., 2006; Reston, 2009; Sutra and Manatschal, 2012). The schematic model of this type of margin development (Figure F4) guided the drilling strategy of Expeditions 367, 368, and 368X. Huismans and Beaumont (2008, 2011) also suggested, however, that final plate rupture can occur without exhumation of the subcontinental mantle and can be followed rather quickly by igneous ocean crust formation, a scenario that our chosen drilling strategy also tested. Therefore, the highly extended northern margin of the SCS is an excellent location to examine whether this margin endured magmatism during breakup or whether its development is closer to the Iberia-type amagmatic margin.

Geological setting

The SCS is a modestly sized young ocean basin that formed along the eastern boundary of the Eurasian plate during the mid-to late Cenozoic (Figure F1). Expeditions 367, 368, and 368X cored and logged a transect of drill sites across the COT in the northern SCS (Figure F5).

The continental crust that was rifted to form the SCS was accreted to the Asian margin during the Mesozoic (Zhou and Li, 2000; Zhou et al., 2008; Li et al., 2012a, 2012b). This relatively young continental lithosphere underwent extensive rifting that started ~80 My later during the Paleogene (Eocene to early Oligocene). Seafloor spreading in the eastern part of the SCS started during the Oligocene, and the oldest magnetic anomaly in the area of the drilling transect is interpreted to be Anomaly C11 (~29.5 Ma) or C12n

Figure F4. A–D. Schematic development of continental breakup initiated by a simple shear along a deep, low-angle fault. B–D are slightly modified from Huismans and Beaumont (2011) and illustrate modeling-based stages of extension at magma-poor, Iberia-Newfoundland type rifted margins. Key features of D: thinning of the upper crust and juxtaposition of lower crust with serpentinized mantle between the outer margin and igneous oceanic crust. UP = upper plate, LP = lower plate. The Expedition 367, 368, and 368X drilling strategy was designed to sample and test whether or not these fundamental crustal units and tectonic relationships are present at the northern South China Sea rifted margin.



(~31 Ma) (Briais et al., 1993; Li et al., 2013, 2014; Franke et al., 2013). Seafloor spreading in the southwest SCS started at ~23 Ma and even later in the most southwestern basin (Briais et al., 1993; Barckhausen and Roeser, 2004; Li et al., 2012a, 2012b; Franke et al., 2013).

The initial half-spreading rate was \sim 3.6 cm/y. It later slowed to 1.2 cm/y, and seafloor spreading eventually ceased by \sim 15 Ma (e.g., Li et al., 2014). The initial spreading rate in the SCS basin, therefore, appears to be higher than the ultraslow spreading off the Iberia-Newfoundland margin (Dick, 2003). Subduction of the eastern part of the SCS basin started at or before \sim 15 Ma along the Manila Trench (Li et al., 2013). For a complete review of the regional setting and tectonic development of the SCS, see Shi and Li (2012), Franke et al. (2013), Li et al. (2013), and Sun et al. (2014).

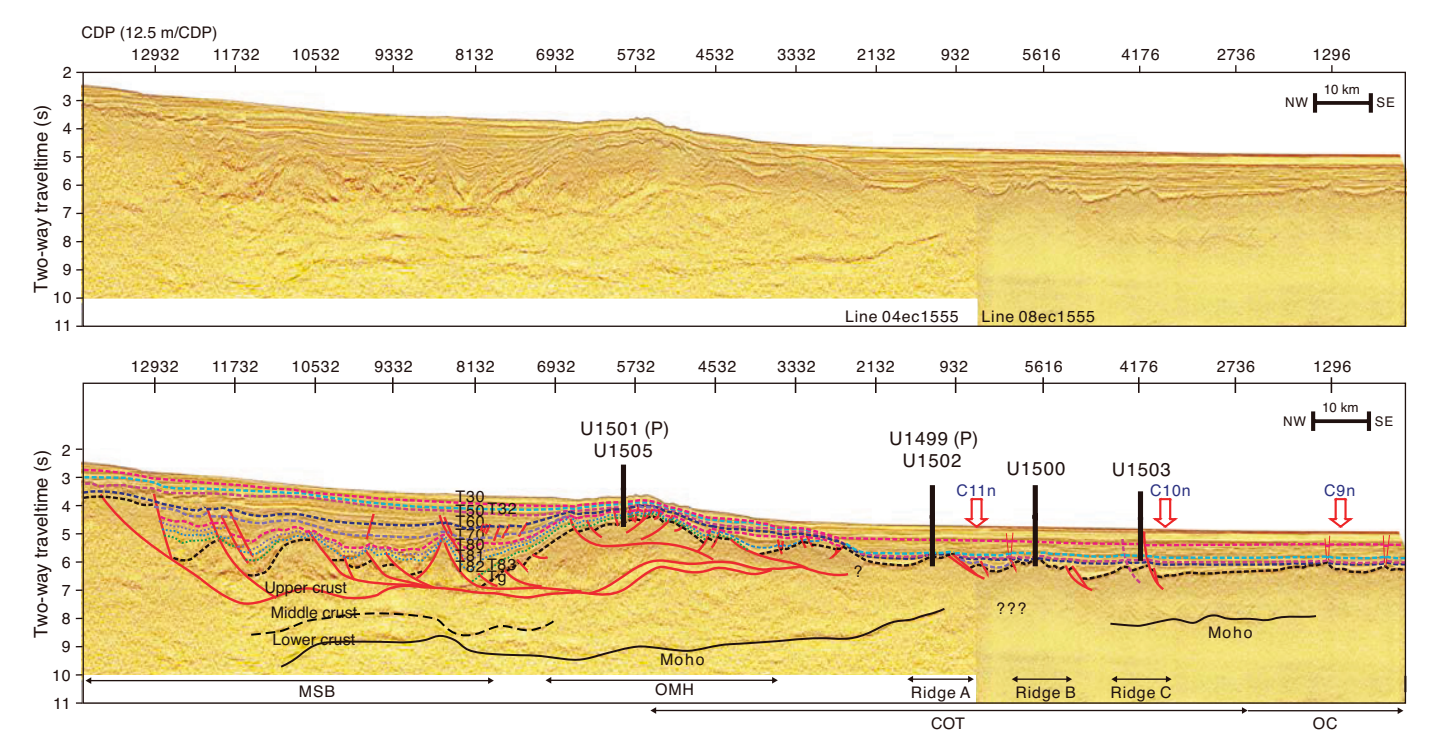
The Expedition 367, 368, and 368X drilling transect is located ~50 km west of IODP Site U1435 (Figures **F1**, **F4**, **F5**) (Li et al., 2015a, 2015b) along a segment of the northern SCS margin bounded to the west by a transform fault. This margin segment exhibits a broad zone of extended crust (COT) (Figure **F5**) that may end to the east somewhere between IODP Sites U1432 and U1435. East of this segment, continental crust seems to transition into ocean crust in a narrower COT.

The segment of the SCS margin investigated during Expeditions 367, 368, and 368X is therefore characterized by a broad COT (~150 km) resulting from intense crustal stretching and extension before breakup. A deep sag basin (midslope basin [MSB]) of presumed Eocene to Oligocene age is present in the midslope area (Figure F5) and is bounded seaward by an outer margin high (OMH) forming a quite persistent structure along the margin to the east. Three distinct ridges (A, B, and C from north to south in Figures F2, F5) are found seaward of the OMH in the more distal margin, representing progressively thinner continental crust in the COT or ocean crust. We refer to the continent/ocean boundary (COB) as the narrow zone in which the outermost, highly thinned continental lithosphere is replaced seaward by new crust that formed at a narrow spreading ridge in a steady-state fashion. The latter can include continuous tectonic exhumation of lithospheric mantle (e.g., Dick et al., 2003), accretion of normal igneous oceanic crust, or a mixture of these two processes. The nature and precise location of the COB at the SCS cannot be interpreted with confidence from the seismic data, and interpretation therefore requires drilling control.

The clear seismic reflections from the Mohorovičić seismic discontinuity (Moho) show distinct thinning of the continental crust (Figure F5) across the COT with a thickness of ~6 km around its seaward end. Separate layers hypothesized to be upper, middle, and lower crust are distinguished in the landward part of the seismic profiles. The lower crust is acoustically transparent and may be as thin as ~6 km in places. Lower crust with a similar thickness and seismic appearance was reported from the northeastern SCS margin (McIntosh et al., 2013, 2014; Lester et al., 2013). The seaward continuation of this crustal layering into the COB zone is ambiguous, however, and prevents us from interpreting the exact location and detailed nature of the COB.

The upper crust shows numerous extensional faults soling out at low-angle detachment faults in the midcrustal level. This fault system generated many deep half-grabens filled with synrift sediments that were subsequently covered by postrift sediments. The boundary between synrift sediments and postrift sediments most often follows the T70 seismic stratigraphic unconformity (Figure F5). Results from distant industry wells as well as those of IODP Site U1435 suggest a breakup unconformity age of ~34 Ma (Li et al., 2015b). However, the time of crustal extension is not necessarily synchro-

Figure F5. Deep crustal time-migrated seismic reflection data without and with interpretation. Note the rather thin lower crust (two layers) above a strong Moho reflector that can be followed oceanward. Moho reflection is weak to absent seaward from around the middle of the interpreted COT. Wide-angle seismic data (Yan et al., 2001) confirm ~6 km thick ocean crust (OC) seaward of the COT. A large detachment fault ~150 km inland of the COT separates more stable crust landward from that of highly extended crust seaward. An OMH is a fairly consistent feature along this margin segment. Key seismic unconformities are shown in purple (T70; ~32 Ma breakup unconformity?) and blue (T60; ~23 Ma regional basin event). These ages are inferred from long-distance (>100 km) correlation of seismic unconformities with industry holes and ODP Leg 184 Site 1148 (T60); they need confirmation by coring and are only tentative. Tg reflector (green) = basement. Arrows and labels C11n, C10n, and C9n = approximate position of seafloor magnetic anomalies with chron numbers (from Briais et al., 1993). Seismic data are from Line 04ec1555-08ec1555 (courtesy of the Chinese National Offshore Oil Corporation [CNOOC]). Location of line is shown in Figures F2 and F3. CDP = common depth point. P = projected location of drilling site onto the seismic profile.



nous across the margin and could be younger toward the outer margin. A younger, widely distributed unconformity (T60) is also observed (Figure F5). The T60 unconformity corresponds to a hiatus at ~23 Ma found at ODP Site 1148 (Wang, Prell, Blum, et al., 2000) and Site U1435 and is approximately synchronous with a southward jump and change in kinematics of the SCS spreading axis and with the breakup in the southwest part of the basin (Briais et al., 1993).

The OMH hosts many relatively shallow half-graben basins on top of this broad basement high. The stratigraphy of these smaller basins can be traced seismically into the deeper, central basin sag below the MSB (Figure F5). The normal faults bounding the OMH basins are clearly imaged and for the main part dip landward. The small rift basins therefore offer an opportunity to sample the stratigraphy covering the entire period of rifting and postrift subsidence. The MSB itself is bounded landward by major, seaward-dipping normal fault(s) that seemingly form major detachments soling out at middle to lower crustal levels but not penetrating through the lower crust. If true, this suggests decoupling between the upper and lower crust and that, at least in this more landward part of the margin, faults never penetrated the lower crust.

The interpretation of some seismic profiles suggests that the lower crust in the COT may thicken seaward, but this observation is not well constrained (Figure F5). Likewise, seismic imaging of the low-angle faults and detachments in the landward part of the COT cannot with confidence be traced into the distal margin regime. One possibility is that the main detachment zone was located above

what later became Ridge A, effectively implying that Ridge A is a core complex consisting of lower continental crust and possibly subcontinental mantle depending on how deeply detachments exhumed the lithosphere in the distal margin. Alternatively, if the main detachment underlies Ridge A, the latter would represent upper plate material of upper crustal origin.

Ridge A is domelike for the most part and shows neither small normal faults nor developed synrift half-grabens like the OMH. Excluding sediment and using the ocean-bottom seismometer (OBS) velocity constraints of Yan et al. (2001), Wang et al. (2006), and Wei et al. (2011), the crust below this outermost basement high is estimated to be only ~6–8 km thick. Seaward of Ridge A, the crust has a fairly uniform thickness of ~6 km, which could be consistent with oceanic crust (Yan et al., 2001; Li et al., 2014). The projection on the seismic profile of the magnetic lineation interpreted to be Anomaly C11 (Briais et al., 1993) coincides with the seaward part of Ridge A (Figures F2, F3, F5).

Both Ridges B and C consist of faulted blocks rotated landward along seaward-dipping normal faults, some of which may be seismically traced to near the base of the crust. Ridge B also shows subhorizontal features on the along-strike seismic profile in the uppermost crust that could be consistent with a volcanic origin. However, these features could also be consistent with a tilted fault block of upper continental crust (i.e., a distal extensional rider of upper plate origin). If this is the case, prerift deposits could be present beneath the seismic unconformity defining the top of acoustic basement at Ridge B. The seismic layered structure of Ridge B

makes it less likely to consist of lower crust or serpentinized mantle. In many ways, Ridge C is seismically similar to Ridge B. However, the significant amplitude of the magnetic anomalies strongly suggests that Ridge C is indeed partial if not full igneous ocean crust.

Sampling the basement at Ridges A, B, and C was therefore essential for the SCS margin science program to distinguish among different tectonic models for breakup along highly extended margins. Ridges A and B help constrain the style of rifting. In contrast, Ridge C is assumed to represent the early igneous crust. The material recovered here will address another key objective of the SCS margin science program: to constrain the nature of early oceanic crust formation. Specifically, we hope to determine how quickly a steady-state igneous system was established, what mantle source is involved (e.g., composition, temperature), what conditions of mantle melting (degree and depth of melting) were present, and what continental crustal contamination of the igneous material, if any, was derived from the asthenospheric mantle.

Expedition objectives

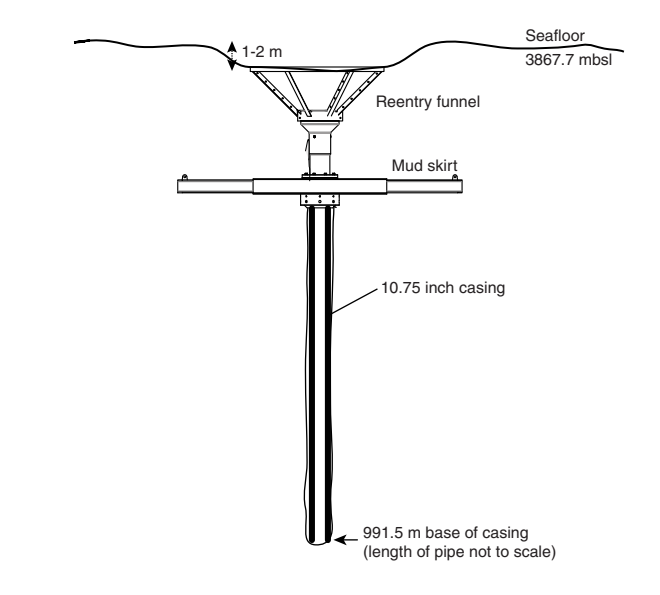
By drilling a transect across the SCS margin, expedition scientists set out to understand the timing and process of rifting, eventual rupturing of the continental crust, and onset of igneous oceanic crust at a highly extended rifted margin (Figure F4). Four primary and sixteen alternate drill sites across a ~150 km wide COT zone were defined in the *Scientific Prospectus* (Sun et al., 2016b). The four primary sites were planned to target the four main tectonic features: the OMH (and its small rift basins) and the three basement ridges (A, B, and C) in the distal margin. At each of these sites, the nature of the acoustic basement and the record of synrift and post-rift deposits were key targets.

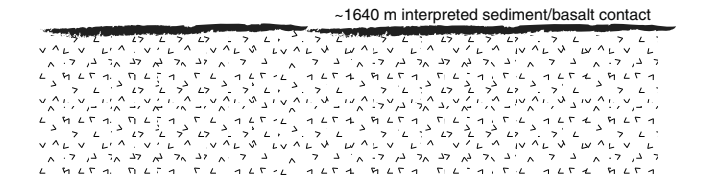
As part of the SCS margin science program, Expedition 368X was planned to complete operations at Hole U1503A. The primary operational objective at Site U1503 was to sample the lowermost ~300 m of sediments on top of basement and at least 100 m of the igneous basement. The sedimentary target will constrain the age and subsidence history of the crust at this location, the timing of normal faulting, and the environment of the early half-graben fill. The basement objective will provide a deep representative sampling of the basaltic material at this site and an important reference frame for the modeling of breakup. Although logging (triple combination [triple combo], Formation MicroScanner [FMS]-sonic, and VSI tool strings) into the basement was originally planned, the condition of Hole U1503A deeper than ~1300 m was unstable and not suitable for logging. Logging deeper than 991.5 m (bottom of casing) was not possible because of unstable hole conditions, but Hole U1503A was logged with the VSI in the cased portion of the hole.

Coring and logging strategy

Drilling operations were based on the original plans for Expedition 368, which were to core and log through thick sediment sections and, significantly, into underlying basement using casing in the upper, unstable part of the sedimentary section. The operational approach was to reenter Hole U1503A using the reentry system and 991.5 m of 10¾ inch casing installed during Expedition 368 (Figure F6).

Figure F6. Expedition 368 reentry system and casing installation, Hole U1503A.

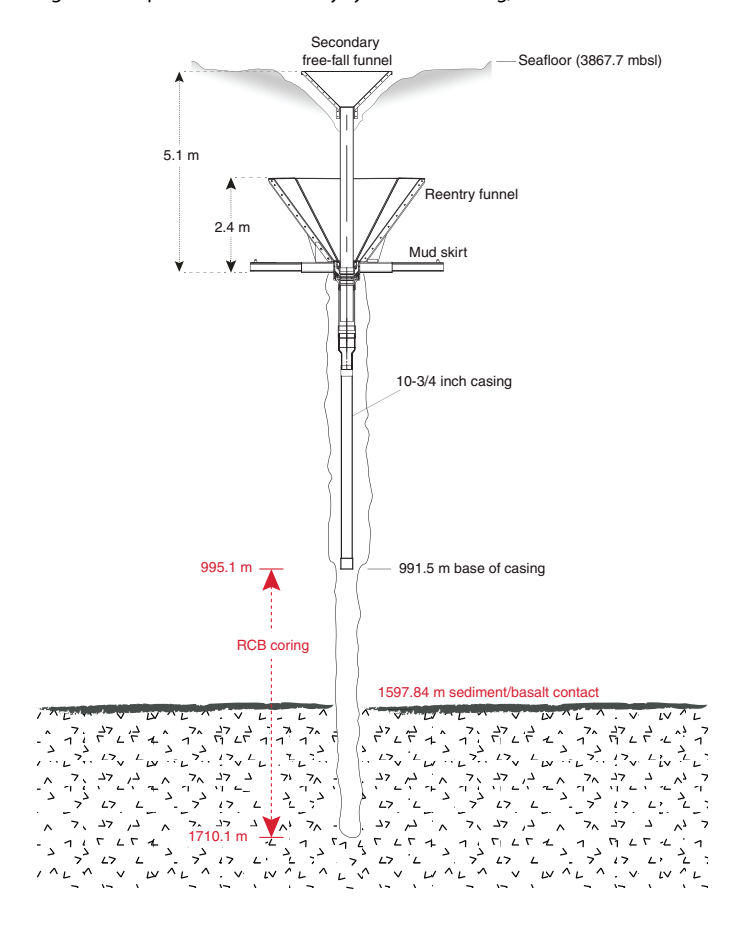




Hole U1503A was designed for coring using the RCB system to extend from the base of the casing through the sediments and into the underlying basement. Multiple pipe trips to replace hard rock RCB bits would be required by the depth of targets within basement. Upon completion of the coring objectives, the RCB bit was to be dropped either in the bottom of the hole or on the seafloor before downhole wireline logging data could be collected. For this deeper logging, we planned to use the triple combo and FMS-sonic tool strings and the VSI tool string to conduct check shots.

During Expedition 368X, we had to modify this general operational plan in response to borehole conditions and the need to focus our operations time to achieve our highest priority basement objective. The reentry cone installed during Expedition 368 was observed to be slightly below the level of the seafloor and full of debris from previous drilling in Hole U1503A. Thus, we installed a secondary free-fall funnel with a 2.7 m extension into the reentry system to ensure our ability to reenter Hole U1503A during multiple pipe trips to replace RCB bits (see **Operations**). RCB coring from 995.1 m (below the casing) to 1710.1 m penetrated 602.74 m of sediments and 112.26 m of basement (Figure F7). We then tripped pipe out of the hole, dropped the bit on the seafloor, and reentered Hole U1503A. Logging deeper than 991.5 m was not possible because of unstable hole conditions, so Hole U1503A was logged with the VSI in the cased portion of the hole (end of casing at 991.5 m).

Figure F7. Expedition 368X reentry system and casing, Hole U1503A.



Site U1503 summary

Background and objectives

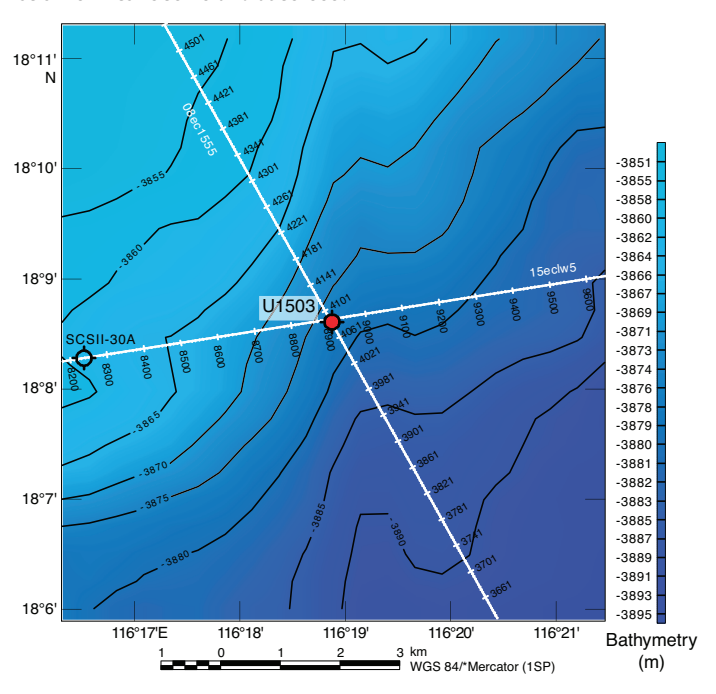
Site U1503 (proposed Site SCSII-9B) is located at 3867.7 m water depth near the top of the structural high named Ridge C (Figures F5, F8; Table T1). Ridge C is the most seaward ridge of the three margin-parallel basement ridges that characterize the lower continental slope underlain by thin (5–7 km) crust and possibly the oldest oceanic crust. Ridge C is believed to represent at least partial if not full oceanic igneous crust and therefore to have formed after the completion of continental breakup along this margin segment of the northern SCS.

A key operational objective of Site U1503 was to sample the lowermost ~300 m of sediments on top of basement to constrain the age and subsidence history of the crust at this location, the timing of normal faulting, and the environment of the early sediment infill. The other critical goal was to sample the igneous stratigraphy to at least 100 m below the acoustic basement. A deep representative sampling of the basaltic material at this site will provide an important reference frame for the modeling of continental breakup and early oceanic spreading. With an estimated sediment thickness of 1640 m overlying basement, obtaining basement samples and log data at this site represented a challenging operation.

Operations

Operations were conducted in one hole at Site U1503 (Table T1). In Hole U1503A, the reentry system and 10¾ inch casing (to 991.5 m) installed during Expedition 368 were used to reenter the

Figure F8. Bathymetry at Site U1503 and location of the site in relation to seismic Lines 15eclw5 and 08ec1555.



existing hole. The RCB system cored from 995.1 to 1597.84 m (602.74 m penetration; 128.01 m recovered; 21%) and then continuously cored 112.26 m into the underlying basalt from 1597.84 to 1710.1 m (47.91 m recovered; 43%). Logging with the VSI tool string was conducted within the casing only.

Lithostratigraphy, igneous and metamorphic petrology, and structural geology

Site U1503 is divided into four lithostratigraphic units (Figure F9); three units are composed of sediments, and one unit consists of igneous basement. The uppermost 995.1 m of sediments were drilled without coring during Expedition 368. Lithostratigraphic Unit I (995.10-1484.74 m) is a 489.6 m thick sequence of well consolidated to lithified brownish gray, moderately bioturbated claystone with greenish gray sandstone and siltstone interbeds (Figure **F10**). Some of the coarser intervals have high carbonate content and multiple sedimentary structures (mud clasts, a fining-upward sequence, and parallel and convolute laminations) that are potentially related to deep-sea turbiditic flows. The relatively low recovery (21%) of Unit I is attributed to the presence of thick sandstone layers that are inferred from the high-amplitude reflectivity of seismic section. Unit II (1484.74-1542.77 m) is divided into Subunits IIA (1484.74-1533.60 m) and IIB (1533.60-1542.77 m) based on carbonate and nannofossil contents. Subunit IIA has a recovery of 36% and consists of lithified dark reddish brown massive claystones with greenish gray intervals containing heavier bioturbation. Subunit IIB has extremely low recovery (3%) and consists of lithified reddish brown clay-rich chalk. The separation of Subunits IIA and IIB is also based on geochemical data. Subunit IIA has low carbonate content and high Sr, Fe, Ni, Zn, and Al concentrations, whereas Subunit IIB is carbonate rich and low in Sr, Fe, Ni, Zn, and Al. Unit III (1542.77-1597.84 m) contains heavily bioturbated lithified greenish gray nannofossil-rich claystone, greenish gray claystone, light greenish gray siltstone, and dark gray banded claystone. Recovery in Unit III is extremely low (5%). A 4 cm thick greenish black interval

Table T1. Operations summary, Expedition 368X Site U1503. Download table in CSV format.

Hole	Proposed site	Location	Water depth (m)	Total penetration (m)	Cored interval (m)	Drilled interval without coring (m)	Core recovery (m)	Core recovery (%)	Time on hole (days)	Cores (N)	Depth of 10-3/4 inch casing (m)	Start date (2018)	Start time UTC (h)	End date (2018)	End time UTC (h)
U1503A	SCSII-9B	18°8.6300′N 116°18.8456′E	3867.7	1710.1	715	0	175.73	26	18.5	87	991.5	18 Nov	1700	7 Dec	0745

Figure F9. Lithostratigraphic summary, Hole U1503A.

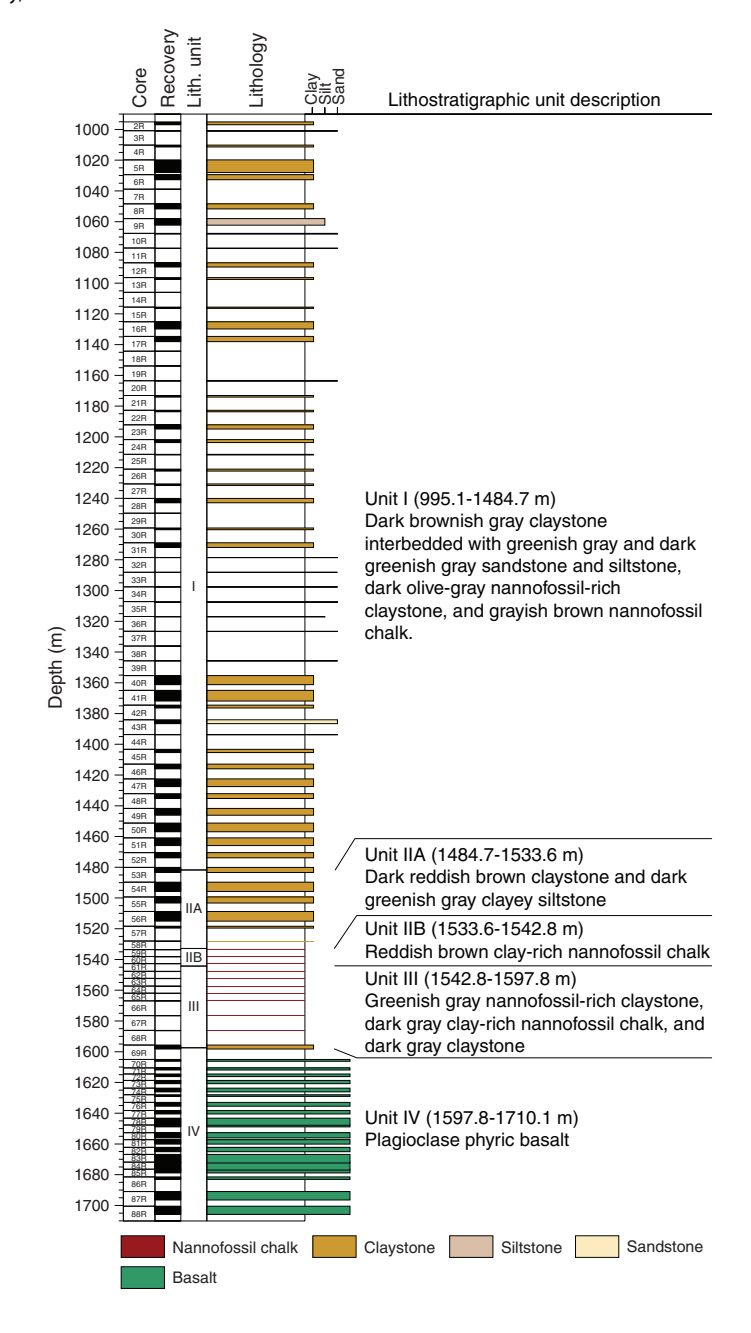
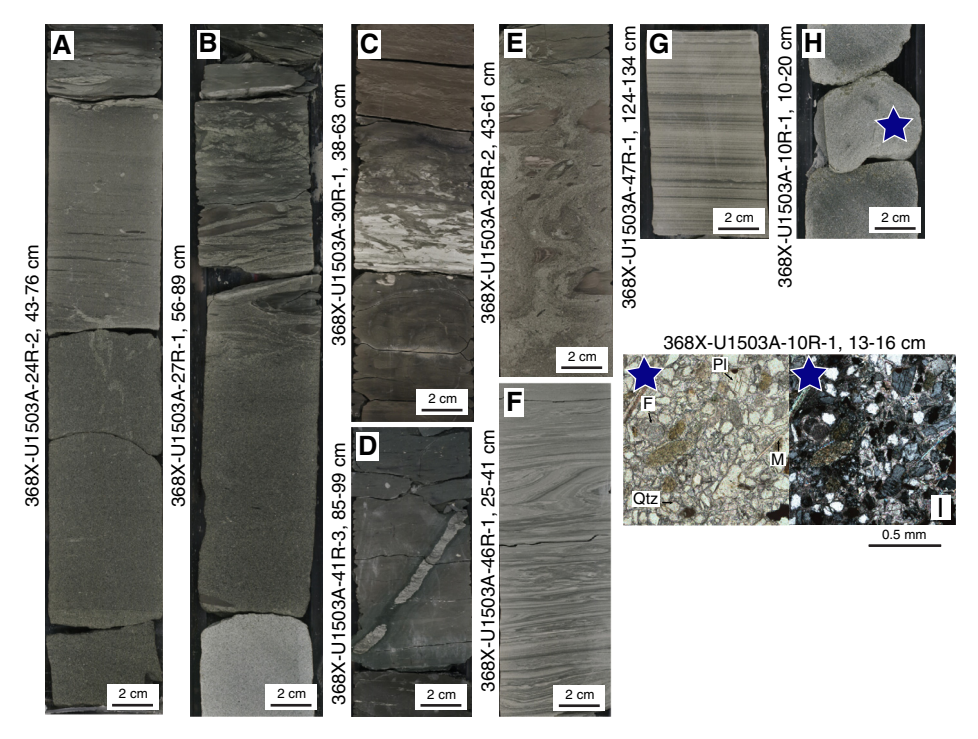


Figure F10. Sedimentary structures from Unit I, Hole U1503A. A. Fining-upward sequence from massive medium-grained sandstone to laminated silty fine-grained sandstone. The sequence is overlain by the planar base of the next fining-upward interval. B. Dark brownish gray laminated clayey siltstone with sand over dark greenish gray sandstone with a low carbonate content. This lithology is underlain by greenish gray sandstone with a high carbonate content. The laminated clayey siltstone with sand has claystone intraclasts. C. Two fining-upward sequences with claystone overlain by laminated clayey siltstone, laminated silty claystone, and claystone. The laminated clayey siltstone has a sharp base that overlies the claystone. The intensity of bioturbation increases upward in the fining-upward sequence. D. Inclined burrow filled with light gray silty sediment cutting across olive-gray, highly bioturbated claystone. E. Sandstone with claystone intraclasts overlain by claystone. F. Convolute and plane laminations in silty fine sandstone. G. Parallel laminations in fine sandstone. H. Greenish gray massive and well-sorted sandstone. Blue star = location of image in I. I. Thin section image of sandstone in H with subangular quartz (Qtz), plagioclase (Pl), muscovite (M), and a foraminifer (F) in carbonate cement.



in Unit III is likely composed of highly altered volcanoclastic material

Lithostratigraphic Unit IV (1597.84-1710.10 m) is an igneous unit that samples the uppermost part of the SCS basement. The boundary between the sediment of Unit III and the underlying basalt of Unit IV at 1597.84 m is unfortunately disturbed by drilling and corresponds to the separation between claystone and basalt rubble at the bottom of the core. Unit IV continues through 112.26 m of basement, of which 47.91 m was recovered. Unit IV is composed primarily of sparsely plagioclase to plagioclase phyric basalt with no vesicles to high vesicle content (Figure F11). Basalts have mostly ophitic to subophitic texture with euhedral phenocrysts of plagioclase. This basalt unit contains chilled margins with preserved fresh glass that are imbricated with clayey sediments or recrystallized carbonate. Veins occur throughout Unit IV and are predominantly filled with carbonates, Fe oxides, chlorites, and zeolites. Alteration of these basalts remains generally low, as evidenced by minimal alteration of interstitial glass and good preservation of plagioclase. The textures, contacts, and structures of Unit IV suggest emplacement as pillow or lobate lava flows in a subaqueous environment.

Biostratigraphy

Between Sections 368X-U1503A-2R-1 and 48R-CC, a 5 cm whole-round sample from the core catcher of each core was collected on the catwalk by *JOIDES Resolution* Science Operator

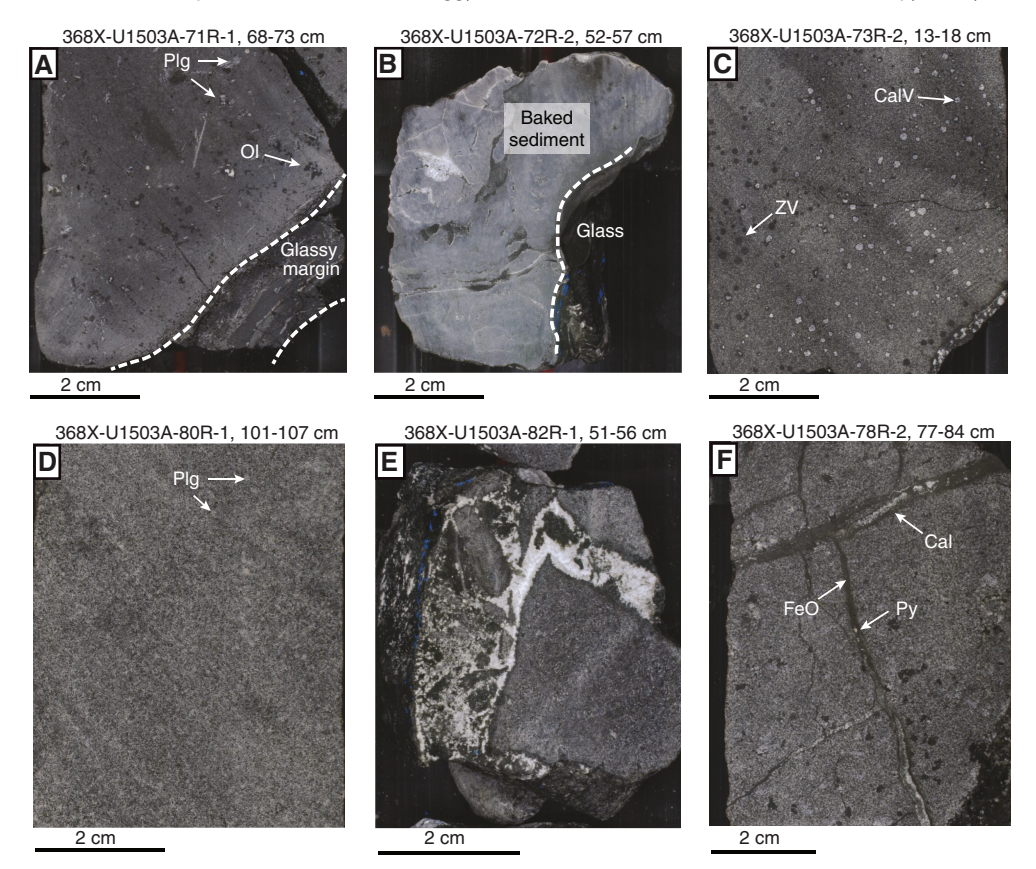
(JRSO) IODP technical staff. The sample was vacuum sealed and stored for shipment to the Gulf Coast Repository (GCR) in College Station, TX (USA), at the end of the expedition. Exceptions to this sampling strategy occurred in particularly low-recovery cores. In lithified sediments and basement, no samples were collected for biostratigraphy deeper than 1441.7 m.

Core catcher samples from Hole U1503A were split at the GCR after Expedition 368X and distributed to members of the Expeditions 367 and 368 micropaleontology team who analyzed them for calcareous nannofossils and planktonic foraminifers. Calcareous nannofossils are barren or rare in most samples, especially in red clay sediments, but are abundant or common in some turbidite or chalk samples. Varying degrees of overgrowth and broken fragments are common on nannofossils. In most parts of the sediment, planktonic foraminifers are barren and moderate to poorly preserved.

Nine biostratigraphic datums were used to provide an age-depth model for Site U1503 from the early Oligocene to the middle Miocene. The early/late Oligocene boundary was placed tentatively between Cores 368X-U1503A-60R and 65R. The early/middle Miocene boundary was determined to occur between Cores 53R and 54R. Sedimentation rates varied from ~7 mm/ky during the Oligocene and early Miocene to ~60 mm/ky in the middle–late Miocene.

Deepwater agglutinated benthic foraminifers were found in Samples 368X-U1503A-26R-CC to 65R-CC, indicating an abyssal paleoenvironment.

Figure F11. Macroscopic features in igneous lithologic Unit 1, Hole U1503A. A. Moderately plagioclase (Plg)-olivine (Ol) phyric basalt with an altered glassy chilled margin. B. Baked blueish gray chert with some glass residue on its side. C. Macroscopic vesicles filled by recrystallized carbonate (CalV) and zeolite (ZV). D. Sparsely Plg phyric basalt with porphyritic texture (most common macroscopic texture observed throughout lithostratigraphic Unit IV). E. Vein with angular basalt fragments in calcite cement. F. Composite vein network with vuggy texture and carbonate (Cal), Fe oxide (FeO) and pyrite (Py) infill.



Paleomagnetism

The intensity of the natural remanent magnetization in sediments at Site U1503 is higher in the reddish claystone (10^{-2} A/m) of lithostratigraphic Unit II than in the brownish, greenish, and gray sediments of both lithostratigraphic Units I (10^{-3} A/m) and III (10^{-4} A/m) . In the basalts (Unit IV), the average initial intensity is at least two to four orders of magnitude higher than in sediments (1 A/m).

Both sediments and basalts can show two components of magnetization:

- A component isolated at lower fields that, at least in sediments, shows steep positive inclination and can be correlated to drilling overprinting and
- A characteristic component of magnetization (characteristic remanent magnetization [ChRM]) that shows both reversed and normal polarities and can be isolated in different field ranges depending on the coercivity of the magnetic carries.

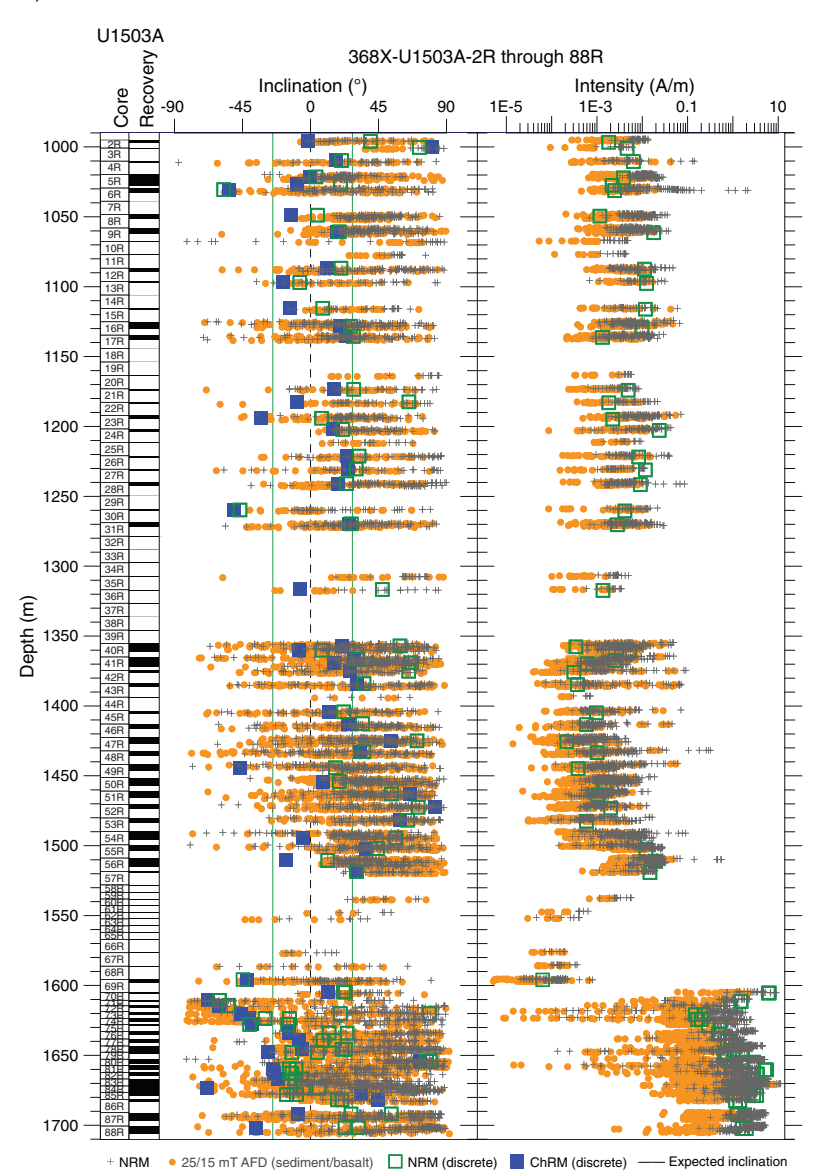
In sediments, the presence of both normal and reversed polarities and a mean ChRM inclination of 26.4° ± 8.0° (close to the 25° inclination expected at the coordinates of Hole U1503A) support a primary nature of the magnetization. However, the observed inclinations (Figure F12) cannot be correlated with a reference geomagnetic polarity timescale because of the extremely low recovery rate.

The anisotropy of magnetic susceptibility shows strong oblate shape and horizontal planar fabric in sediments, which is consistent with deposition in a calm pelagic environment. An inclined planar fabric is present in lithostratigraphic Units II and III and shows a foliation inclined by $\sim\!30^\circ$. In basalts, a prolate shape of the ellipsoid and an intermediate fabric indicate the presence of a flow; however, the flow direction cannot be determined because samples are not oriented.

Geochemistry

Geochemical analyses were conducted for headspace gas safety monitoring in all sediment cores and two basement cores. Methane content is low (<30 ppmv) in the sediment sections shallower than 1394 m. Deeper than 1404 m, methane content in sediments gradually increases (average = 1249 ppmv) before reaching a maximum of 5066 ppmv very near the sediment/basement boundary. Quantification of sediment $CaCO_3$, inorganic and organic carbon, nitrogen, and sulfur contents was made for 43 samples (Figure F13). Samples with carbonate content >30 wt%, from near the top of the cored sediments, correspond to sandstones in lithostratigraphic Unit I. With three exceptions, total organic carbon (TOC)/total nitrogen (TN) ratios at Site U1503 range from <1 to 6.4 (average = 4.3; Figure F13), suggesting that the majority of the organic matter is likely from a marine source. Source rock analysis was performed on three sedimentary samples. Samples collected for X-ray diffraction analysis

Figure F12. Magnetic measurements, Hole U1503A.



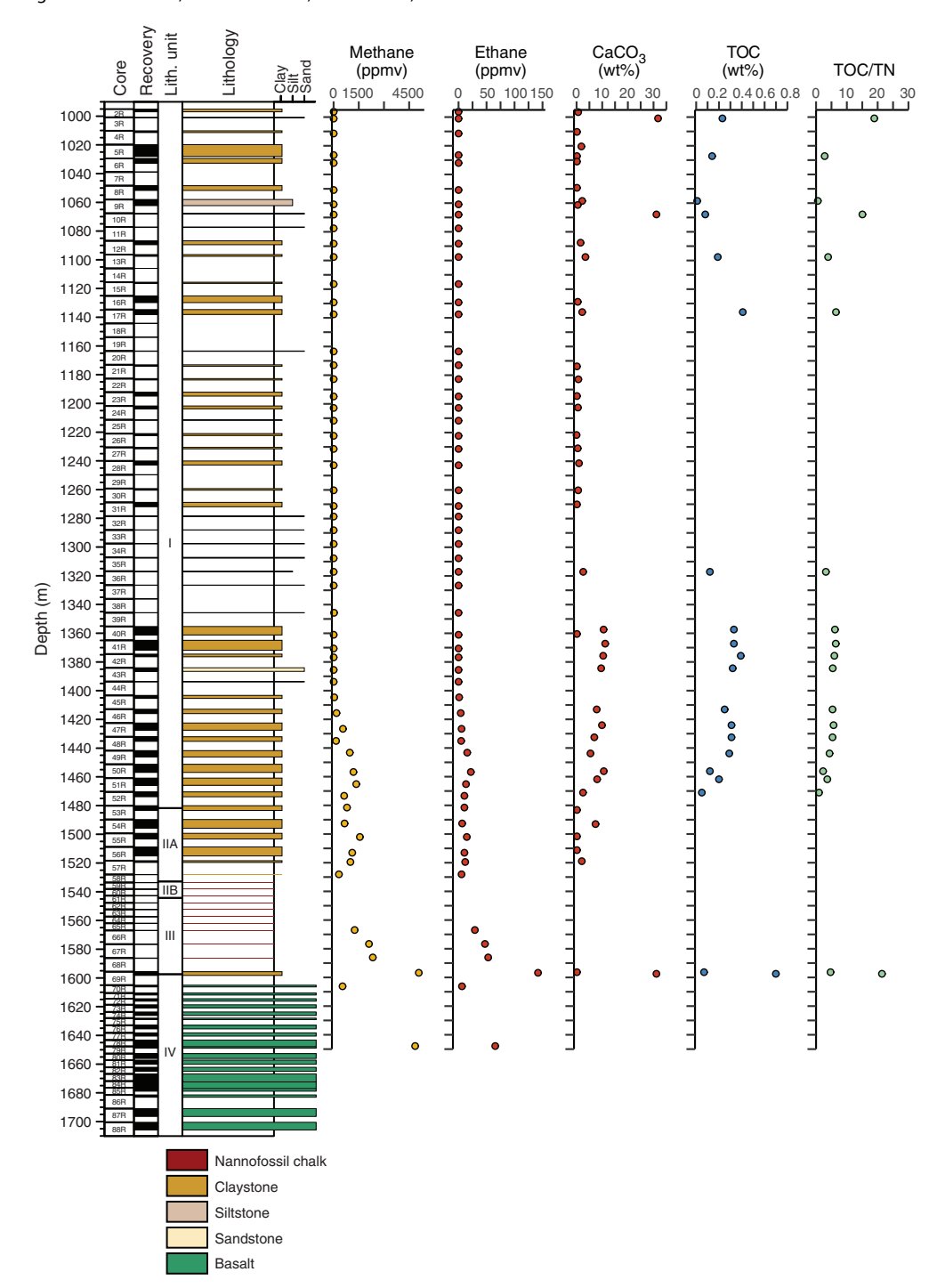
(see the **Expedition 367/368 methods** chapter [Sun et al., 2018]) were retained for shore-based analysis of major element oxides and several trace elements using inductively coupled plasma—atomic emission spectroscopy.

Physical properties

We measured physical properties on whole-round cores, working-half sections, and discrete samples. These measurements included gamma ray attenuation bulk density, magnetic susceptibility, natural gamma radiation (NGR), *P*-wave velocity, moisture and density (MAD) and porosity, and thermal conductivity. The variations in physical property values led us to define physical properties (PP) Units 1–9, each of which has specific characteristics (Figure F14). Lithostratigraphic Unit I includes PP Units 1–5. Subunit IIA includes PP Units 6 and 7. Subunit IIB and Unit III correspond to PP Unit 8. Unit IV corresponds to PP Unit 9. In PP Unit I, variations of physical properties are mostly related to the nature of the sediment; NGR, magnetic susceptibility, and porosity are higher, and density, *P*-wave velocity, and thermal conductivity are lower in the claystone

and siltstone than in the sandstone. The P-wave velocity of the claystone and siltstone also increases slightly with depth because of lithification. In PP Unit 7, magnetic susceptibility increases markedly in the red clay of Subunit IIA. The nannofossil-rich claystone of Unit III, which corresponds to PP Unit 8, displays a clear decrease in bulk density, magnetic susceptibility, and P-wave velocity with depth. Such variations, which are opposite to those expected from lithification or compaction effects, are possibly due to the abundance of nannofossils in the sediment. Magnetic susceptibility in the basalts is very high but shows some variations that might correspond to changes in the nature of the magnetized minerals or the grain size. Compared to the sedimentary rocks above the basement, P-wave velocity in the basalts is quite high. NGR (<10 counts/s) and porosity are quite low in the basalts, whereas density is much higher than in sediment. The high magnetic susceptibility values in Cores 368X-U1503A-87R and 88R correspond to basalts that display more massive textures than those from the other cores and are likely to have distinct magnetized minerals or grain size.

Figure F13. Headspace gas concentration, carbon content, and TOC/TN, Hole U1503A.



Downhole measurements and seismic correlation

A VSI tool string was deployed to collect a vertical seismic profile from 18 stations at 50 m intervals from 974.9 to 124.9 m in Hole U1503A. To avoid potentially deteriorated conditions in the open hole, the VSI tool string did not pass into the open hole; all check shots were conducted inside the casing. The VSI tool string was first lowered to near the end of the casing at $\sim\!991$ m. The logging string was then pulled up and stopped at 18 stations. The VSI tool string was combined with telemetry and gamma ray tools. Following data

collection, logging specialists at the Lamont-Doherty Earth Observatory provided corrected traveltimes. The combined VSI and *P*-wave measurements were used to calculate the velocity-depth relationship for Hole U1503A using the interval velocity from the VSI experiment for the top part and the average *P*-wave velocity of sediment cores. Seismic waveforms in Hole U1503A were then extracted from seismic data and converted to depth using the composite depth-velocity relationship for the hole (Figure **F15**). The boundaries of multiple PP and lithostratigraphic units are connected to the prominent reflectors in the seismic image.

Figure F14. Physical properties summary, Hole U1503A. Note the log scale of magnetic susceptibility (MS). WRMSL = Whole-Round Multisensor Logger.

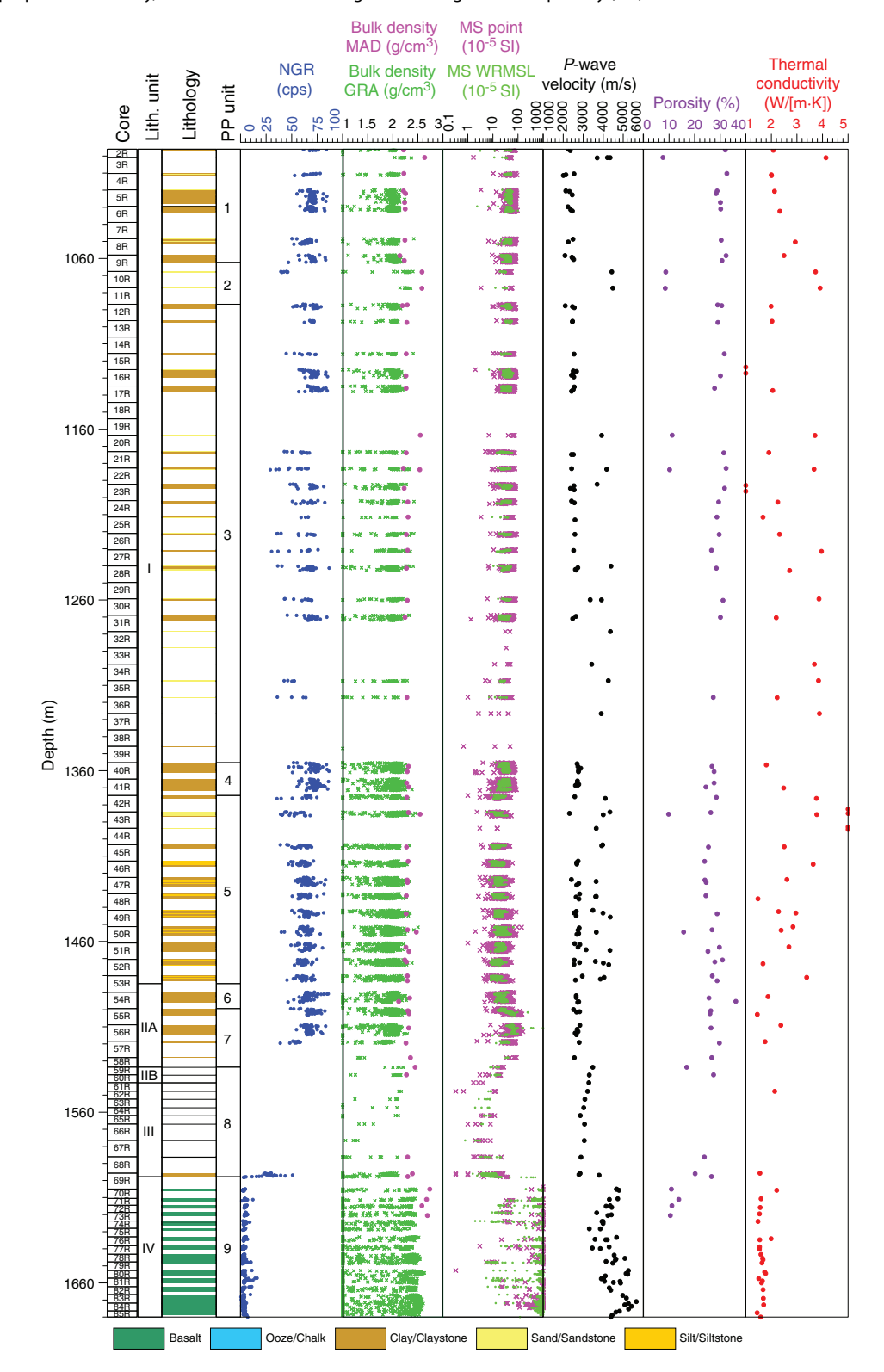
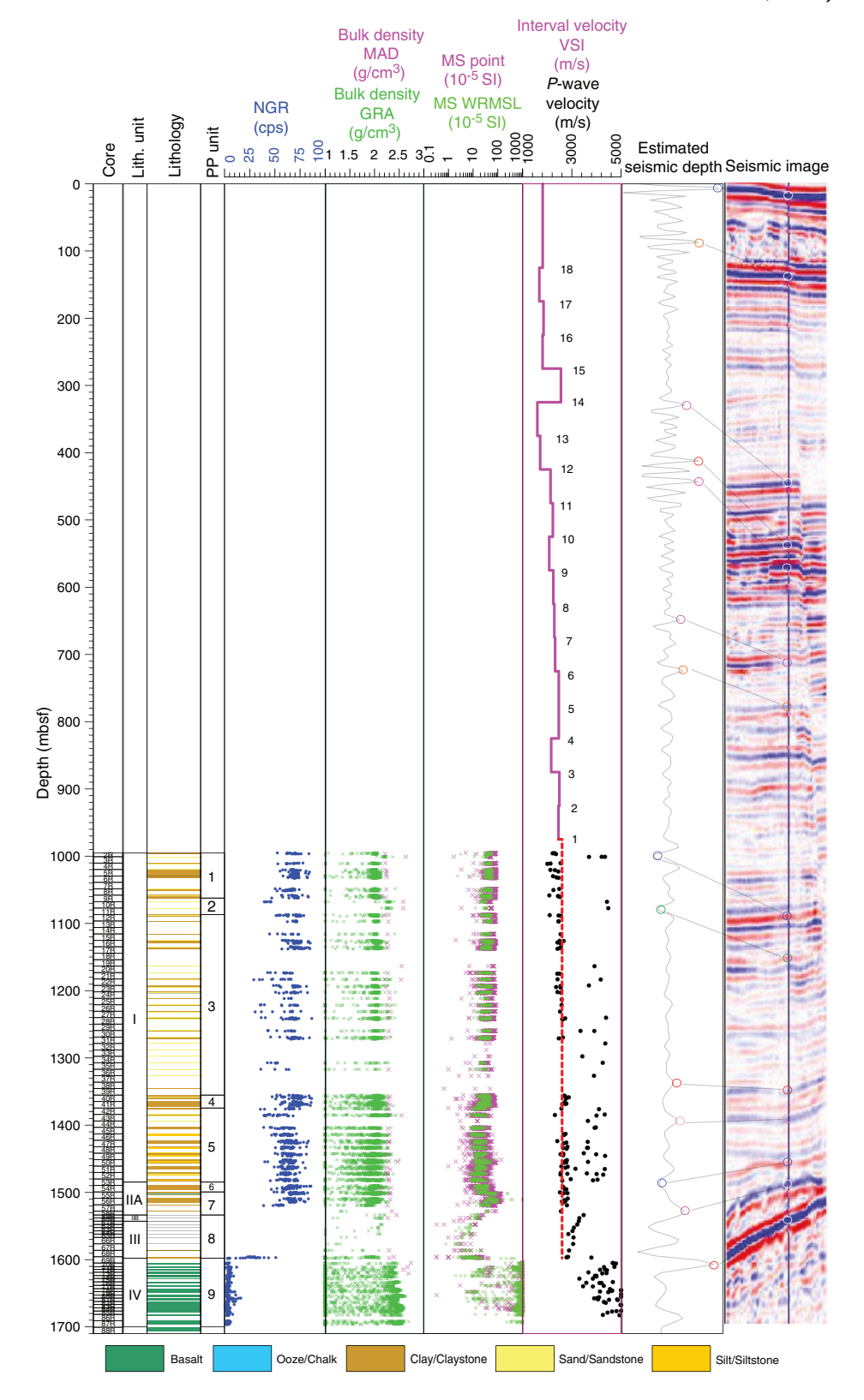


Figure F15. Physical properties and VSI data, Hole U1503A. Red dashed line = average *P*-wave velocity for sediments. Estimated seismic depth is calculated using a composite velocity-depth relationship from the VSI and *P*-wave velocity. Seismic image is not corrected to depth. Open circles and thin black lines connect prominent seismic reflectors to the individual seismic wave forms. Seismic data are from Line 04ec1555-08ec1555 (courtesy of CNOOC).



Preliminary scientific assessment

In this section, we assess the achievements of Expedition 368X in terms of meeting the four specific objectives of Expeditions 367 and 368 as stated in the *Scientific Prospectus* (Sun et al., 2016b). Based on the reentry system and casing installation completed during Expedition 368 and the need to address uncompleted operational objectives, Expedition 368X operated exclusively in Hole U1503A. The drilling strategy for Expedition 368X was to finish the operational objectives of Expedition 368 in Hole U1503A, including coring the lowermost sediments and basement and logging the hole.

1. Determine the nature of the basement within critical crustal units across the COT of the SCS rifted margin to discriminate between different competing models of breakup at magma-poor rifted margins. Specifically, to determine whether the subcontinental lithospheric mantle was exhumed during plate rupture.

This objective was partly achieved during Expedition 368X with the potential for completion following postcruise research.

Site U1503 was a priority deep site on distal Ridge C, as stated in the Scientific Prospectus (Sun et al., 2016b). Expedition 368X penetrated 112.26 m into the basement of Hole U1503A and recovered 47.91 m (43%) of basalt. Although the age of crustal material from Hole U1503A is not yet determined, onboard igneous and metamorphic petrology and structural geology observations were made. The textural and structural features of the basalts suggest an emplacement as pillow or lobate lava flows at the seafloor. Basement in Hole U1503A is composed primarily of sparsely plagioclase to plagioclase phyric basalt. Vesicles are apparent in some intervals, and most samples are ophitic in texture. The basalts contain hypohyaline to holohyaline chilled margins with preserved fresh glass imbricated with clayey sediments. No indication of subcontinental mantle or igneous continental rocks is apparent at Site U1503. Even if the emplacement age of these basalts is not determined yet, we infer that they represent the incipient or steady-state formation of an oceanic crust.

2. Determine the time lag between plate rupture and asthenospheric upwelling that allowed decompression melting to generate igneous ocean crust.

This objective was partly achieved during Expedition 368X, with the potential for completion following postcruise research.

The large recovery of igneous basement rocks at Site U1503 is ideal for geochemical analyses to determine the rock composition, melting process, age of crystallization, or mantle fertility. The combination of such analyses and further geochemical or thermomechanical modeling will constrain the mantle origin and melting processes that lead to the formation of these basalts and potentially reveal if they were emplaced at a steady-state, mature seafloorspreading ridge. Expeditions 367, 368, and 368X sampled basalts at three sites (U1500, U1502, and U1503) that form a 36 km transect across the COT. The accurate measurement of the absolute age of basement formation at each of these sites will be crucial to determine the velocity of continental breakup processes from the first occurrence of mid-ocean-ridge basalt to the steady-state accretion. Comparison of the composition of these basalts with those sampled at Sites U1431 and U1433 during IODP Expedition 349 will also constrain the scenario of breakup to steady-state igneous crust emplacement. These observations and future studies form a unique

data set representing a benchmark for a rifted margin with moderate magmatism that can be compared to the Iberia-Newfoundland magma-poor margin, where a time lag between crustal rupture and onset of seafloor spreading of >15 My has been determined.

3. Constrain the rate of extension and vertical crustal movements.

This objective was partly achieved during Expedition 368X, with the potential for completion following postcruise research.

The inability to pursue coring at Site U1503 prevented Expedition 368 from extending subsidence studies seaward of Ridge B (Site U1500). With the recovered material of Expedition 368X, when the basalts are dated, we will be able to calibrate magnetic models and better identify magnetic isochrons and determine the spreading rate.

4. Improve the understanding of the Cenozoic regional tectonic and environmental development of the Southeast Asia margin and SCS by combining Expedition 367 and 368 results with existing ODP/IODP sediment records and regional seismic data.

This objective was partly achieved during Expedition 368X, with the potential for completion following postcruise research. Contributions include

- Recovery of sandstone that may contain zircons useful for provenance studies to determine the sediment origin (China, Palawan, Taiwan and associated uplift, and Luzon);
- Recovery of red clays that have been observed at most regional sites and record an episode of open-sea, deep-marine conditions. When the Luzon arc started to close the SCS in the east, the SCS was no longer connected with the Pacific Ocean and became a marginal oceanic basin with a different oceanic circulation and sedimentation;
- Observation that the chalk layer of lithostratigraphic Subunit IIB may be regionally correlated;
- Observation that sediments just above the basement are tilted, which can contribute to the dating of faulting at Ridge C; and
- Information regarding the composition and age of formation of the basalts at Site U1503 that, along with results of the previous IODP expeditions, provides unique information on the regional mantle processes during the formation of the SCS and therefore on the geodynamics of Southeast Asia.

References

Barckhausen, U., and Roeser, H.A., 2004. Seafloor spreading anomalies in the South China Sea revisited. In Clift, P., Wang, P., Kuhnt, W., and Hayes, D. (Eds.), Continent-Ocean Interactions within East Asian Marginal Seas. Geophysical Monograph, 149:121–125.

https://doi.org/10.1029/149GM07

Briais, A., Patriat, P., and Tapponnier, P., 1993. Updated interpretation of magnetic anomalies and seafloor spreading stages in the South China Sea: implications for the Tertiary tectonics of Southeast Asia. *Journal of Geophysical Research: Solid Earth*, 98(B4):6299–6328.

https://doi.org/10.1029/92JB02280

Brune, S., Heine, C., Clift P.D., and Pérez-Gussinyé, M., 2017. Rifted margin architecture and crustal rheology: reviewing Iberia-Newfoundland, central South Atlantic, and South China Sea. *Marine and Petroleum Geology*, 79:257–281. https://doi.org/10.1016/j.marpetgeo.2016.10.018

Dick, H.J.B., Lin, J., and Schouten, H., 2003. An ultraslow-spreading class of ocean ridge. *Nature*, 426(6965):405–412. https://doi.org/10.1038/nature02128

Doré, T., and Lundin, E., 2015. Hyperextended continental margins—knowns and unknowns. *Geology*, 43(1):95–96.

https://doi.org/10.1130/focus012015.1

- Franke, D., Savva, D., Pubellier, M., Steuer, S., Mouly, B., Auxietre, J.-L., Meresse, F., and Chamot-Rooke, N., 2013. The final rifting evolution in the South China Sea. *Marine and Petroleum Geology*, 58(Part B):704–720. https://doi.org/10.1016/j.marpetgeo.2013.11.020
- Huismans, R., and Beaumont, C., 2011. Depth-dependent extension, twostage breakup and cratonic underplating at rifted margins. *Nature*, 473(7345):74–78. https://doi.org/10.1038/nature09988
- Huismans, R.S., and Beaumont, C., 2008. Complex rifted continental margins explained by dynamical models of depth-dependent lithospheric extension. *Geology*, 36(2):163–166. https://doi.org/10.1130/G24231A.1
- Lester, R., McIntosh, K., Van Avendonk, H.J.A., Lavier, L., Liu, C.-S., and Wang, T.K., 2013. Crustal accretion in the Manila trench accretionary wedge at the transition from subduction to mountain-building in Taiwan. *Earth and Planetary Science Letters*, 375:430–440. https://doi.org/10.1016/j.epsl.2013.06.007
- Li, C.-F., Lin, J., and Kulhanek, D.K., 2013. Expedition 349 Scientific Prospectus: South China Sea Tectonics. International Ocean Discovery Program. https://doi.org/10.2204/iodp.sp.349.2013
- Li, C.-F., Lin, J., Kulhanek, D.K., Williams, T., Bao, R., Briais, A., Brown, E.A., Chen, Y., Clift, P.D., Colwell, F.S., Dadd, K.A., Ding, W., Hernández-Almeida, I., Huang, X.-L., Hyun, S., Jiang, T., Koppers, A.A.P., Li, Q., Liu, C., Liu, Q., Liu, Z., Nagai, R.H., Peleo-Alampay, A., Su, X., Sun, Z., Tejada, M.L.G., Trinh, H.S., Yeh, Y.-C., Zhang, C., Zhang, F., Zhang, G.-L., and Zhao, X., 2015a. Expedition 349 summary. *In* Li, C.-F., Lin, J., Kulhanek, D.K., and the Expedition 349 Scientists, *South China Sea Tectonics*. Proceedings of the International Ocean Discovery Program, 349: College Station, TX (International Ocean Discovery Program).

https://doi.org/10.14379/iodp.proc.349.101.2015

- Li, C.-F., Lin, J., Kulhanek, D.K., Williams, T., Bao, R., Briais, A., Brown, E.A., Chen, Y., Clift, P.D., Colwell, F.S., Dadd, K.A., Ding, W., Hernández-Almeida, I., Huang, X.-L., Hyun, S., Jiang, T., Koppers, A.A.P., Li, Q., Liu, C., Liu, Q., Liu, Z., Nagai, R.H., Peleo-Alampay, A., Su, X., Sun, Z., Tejada, M.L.G., Trinh, H.S., Yeh, Y.-C., Zhang, C., Zhang, F., Zhang, G.-L., and Zhao, X., 2015b. Site U1435. *In* Li, C.-F., Lin, J., Kulhanek, D.K., and the Expedition 349 Scientists, *South China Sea Tectonics*. Proceedings of the International Ocean Discovery Program, 349: College Station, TX (International Ocean Discovery Program).
 - https://doi.org/10.14379/iodp.proc.349.107.2015
- Li, C.-F., Wang, P., Franke, D., Lin, J., and Tian, J., 2012a. Unlocking the opening processes of the South China Sea. *Scientific Drilling*, 14:55–59. https://doi.org/10.2204/iodp.sd.14.07.2012
- Li, C.-F., Xu, X., Lin J., Sun, Z., Zhu, J., Yao, Y., Zhao, X., et al., 2014. Ages and magnetic structures of the South China Sea constrained by deep tow magnetic surveys and IODP Expedition 349. *Geochemistry, Geophysics, Geosystems*, 15(12):4958–4983.

https://doi.org/10.1002/2014GC005567

- Li, J., Ding, W., Wu, Z., Zhang, J., and Dong, C., 2012b. The propagation of seafloor spreading in the southwestern subbasin, South China Sea. *Chinese Science Bulletin*, 57(24):3182–3191.
 - https://doi.org/10.1007/s11434-012-5329-2
- McIntosh, K., Lavier, L., van Avendonk, H., Lester, R., Eakin, D., and Liu, C.-S., 2014. Crustal structure and inferred rifting processes in the northeast South China Sea. *Marine and Petroleum Geology*, 58(Part B):612–626. https://doi.org/10.1016/j.marpetgeo.2014.03.012
- McIntosh, K., van Avendonk, H., Lavier, L., Lester, W.R., Eakin, D., Wu, F., Liu, C.-S., and Lee, C.-S., 2013. Inversion of a hyper-extended rifted margin in the southern Central Range of Taiwan. *Geology*, 41(8):871–874. https://doi.org/10.1130/G34402.1
- Pérez-Gussinyé, M., Phipps Morgan, J., Reston, T.J., and Ranero, C.R., 2006. The rift to drift transition at non-volcanic margins: insights from numerical modelling. *Earth and Planetary Science Letters*, 244(1–2):458–473. https://doi.org/10.1016/j.epsl.2006.01.059
- Pérez-Gussinyé, M., and Reston, T.J., 2001. Rheological evolution during extension at nonvolcanic rifted margins: onset of serpentinization and development of detachments leading to continental breakup. *Journal of*

Geophysical Research: Solid Earth, 106(B3):3961-3975.

https://doi.org/10.1029/2000JB900325

- Reston, T.J., 2009. The structure, evolution and symmetry of the magma-poor rifted margins of the North and Central Atlantic: a synthesis. *Tectonophysics*, 468(1–4):6–27. https://doi.org/10.1016/j.tecto.2008.09.002
- Shi, H., and Li, C.-F., 2012. Mesozoic and early Cenozoic tectonic convergence-to-rifting transition prior to opening of the South China Sea. *International Geology Review*, 54(15):1801–1828.
 - https://doi.org/10.1080/00206814.2012.677136
- Sun, Z., Jian, Z., Stock, J.M., Larsen, H.C., Klaus, A., Alvarez Zarikian, C.A., Boaga, J., Bowden, S.A., Briais, A., Chen, Y., Cukur, D., Dadd, K.A., Ding, W., Dorais, M.J., Ferré, E.C., Ferreira, F., Furusawa, A., Gewecke, A.J., Hinojosa, J.L., Höfig, T.W., Hsiung, K.-H., Huang, B., Huang, E., Huang, X.-L., Jiang, S., Jin, H., Johnson, B.G., Kurzawski, R.M., Lei, C., Li, B., Li, L., Li, Y., Lin, J., Liu, C., Liu, C., Liu, Z., Luna, A., Lupi, C., McCarthy, A.J., Mohn, G., Ningthoujam, L.S., Nirrengarten, M., Osono, N., Peate, D.W., Persaud, P., Qiu, N., Robinson, C.M., Satolli, S., Sauermilch, I., Schindlbeck, J.C., Skinner, S.M., Straub, S.M., Zu, X., Tian, L., van der Zwan, F.M., Wan, S., Wu, H., Xiang, R., Yadav, R., Yi, L., Zhang, C., Zhang, J., Zhang, Y., Zhao, N., Zhong, G., and Zhong, L., 2018. Expedition 367/368 methods. In Sun, Z., Jian, Z., Stock, J.M., Larsen, H.C., Klaus, A., Alvarez Zarikian, C.A., and the Expedition 367/368 Scientists, South China Sea Rifted Margin. Proceedings of the International Ocean Discovery Program, 367/368: College Station, TX (International Ocean Discovery Program). https://doi.org/10.14379/iodp.proc.367368.102.2018
- Sun, Z., Liu, S., Pang, X., Jiang, J., and Mao, S., 2016a. Recent research progress on the rifting-breakup process in passive continental margins. *Journal of Tropical Oceanography*, 35(1):1–16. (in Chinese with English abstract) https://doi.org/10.11978/2015030
- Sun, Z., Stock, J., Jian, Z., McIntosh, K., Alvarez Zarikian, C.A., and Klaus, A., 2016b. Expedition 367/368 Scientific Prospectus: South China Sea Rifted Margin. International Ocean Discovery Program.

https://doi.org/10.14379/iodp.sp.367368.2016

- Sun, Z., Xu, Z., Sun, L., Pang, X., Yan, C., Li, Y., Zhao, Z., Wang, Z., and Zhang, C., 2014. The mechanism of post-rift fault activities in Baiyun sag, Pearl River Mouth Basin. *Journal of Asian Earth Sciences*, 89:76–87. https://doi.org/10.1016/j.jseaes.2014.02.018
- Sutra, E., and Manatschal, G., 2012. How does the continental crust thin in a hyperextended rifted margin? Insights from the Iberia margin. *Geology*, 40(2):139–142. https://doi.org/10.1130/G32786.1
- Wang, P., Prell, W.L., Blum, P., et al., 2000. Proceedings of the Ocean Drilling Program, Initial Reports, 184: College Station, TX (Ocean Drilling Program). https://doi.org/10.2973/odp.proc.ir.184.2000
- Wang, T.K., Chen, M.-K., Lee, C.-S., and Xia, K., 2006. Seismic imaging of the transitional crust across the northeastern margin of the South China Sea. *Tectonophysics*, 412(3–4):237–245.

https://doi.org/10.1016/j.tecto.2005.10.039

- Wei, X.-D., Ruan, A.-G., Zhao, M.-H., Qiu, X.-L., Li, J.-B., Zhu, J.-J., Wu, Z.-L., and Ding, W.-W., 2011. A wide-angle OBS profile across the Dongsha uplift and Chaoshan depression in the mid-northern South China Sea. *Chinese Journal of Geophysics*, 54(6):1149–1160.
 - https://doi.org/10.1002/cjg2.1691
- Whitmarsh, R.B., Manatschal, G., and Minshull, T.A., 2001. Evolution of magma-poor continental margins from rifting to seafloor spreading. *Nature*, 413(6852):150–154. https://doi.org/10.1038/35093085
- Yan, P., Zhou, D., and Liu, Z., 2001. A crustal structure profile across the northern continental margin of the South China Sea. *Tectonophysics*, 338(1):1–21. https://doi.org/10.1016/S0040-1951(01)00062-2
- Zhou, D., Sun, Z., Chen, H., Xu, H., Wang, W., Pang, X., Cai, D., and Hu, D., 2008. Mesozoic paleogeography and tectonic evolution of South China Sea and adjacent areas in the context of Tethyan and Paleo-Pacific interconnections. *Island Arc*, 17(2):186–207.

https://doi.org/10.1111/j.1440-1738.2008.00611.x

Zhou, X.M., and Li, W.X., 2000. Origin of late Mesozoic igneous rocks in southeastern China: implications for lithosphere subduction and underplating of mafic magmas. *Tectonophysics*, 326(3–4):269–287. https://doi.org/10.1016/S0040-1951(00)00120-7